Optimal switching strategies in multidrug therapies for chronic diseases

Juan Magalang [1,2] Javier Aguilar [3] Jose Perico Esguerra [4] Édgar Roldán [5,*] and Daniel Sanchez-Taltavull [1,†]

[1]*Department of Visceral Surgery and Medicine, Inselspital, Bern University Hospital, University of Bern, Murtenstrasse 35, Bern 3008, Switzerland*

[2]*Institute of Mathematical Statistics and Actuarial Science, University of Bern, Alpeneggstrasse 22, Bern 3012, Switzerland*

[3]*Laboratory of Interdisciplinary Physics, Department of Physics and Astronomy "G. Galilei", University of Padova, Padova, Italy*

[4]*Theoretical Physics Group, National Institute of Physics, University of the Philippines Diliman, Quezon City 1101, Philippines*

[5]*The Abdus Salam International Centre for Theoretical Physics (ICTP), Strada Costiera 11, Trieste 34151, Italy*

(Received 6 December 2024; accepted 29 May 2025; published 10 September 2025)

Antimicrobial resistance is a threat to public health with millions of deaths linked to drug-resistant infections every year. To mitigate resistance, common strategies that are used are combination therapies and therapy switching. However, the stochastic nature of pathogenic mutation makes the optimization of these strategies challenging. Here, we propose a two-scale stochastic model that considers the effective evolution of therapies in a multidimensional efficacy space, where each dimension represents the efficacy of a specific drug in the therapy. The diffusion of therapies within this space is subject to stochastic resets, representing therapy switches. The boundaries of the space, inferred from coarser pathogen-host dynamics, can be either reflecting or absorbing. Reflecting boundaries impede full recovery of the host, while absorbing boundaries represent the development of antimicrobial resistance, leading to therapy failure. We derive analytical expressions for the average absorption times, accounting for both continuous and discrete genomic changes using the frameworks of Langevin and master equations, respectively. These expressions allow us to evaluate the relevance of times between drug switches and the number of simultaneous drugs in relation to typical timescales for drug resistance development. To study realistic therapy scenarios, we impose constraints on the number of administered therapies and/or their costs, which reveals nontrivial optimal drug-switching protocols that maximize the time before antimicrobial resistance develops while reducing therapy costs. Finally, we extend the model to consider single-cell heterogeneity to accurately capture the effects of individual mutations that result in drug resistance.

DOI: 10.1103/htck-mcby

I. INTRODUCTION

Antimicrobial resistance has been recognized as a major threat to public health, with estimates of 4 million deaths associated with resistant bacterial infection in 2019 [1]. This resistance is a consequence of pathogenic evolution, affecting multiple diseases such as tuberculosis [2], HIV/AIDS [3,4], and cancer [5–8], among others. Drug-resistant pathogens are more difficult to treat since conventional treatment procedures can no longer be used. This increases the risk of complications due to more aggressive drugs and the economic burden, with excess costs estimated at 100 000 USD per case of multidrug-resistant tuberculosis in 2013 [9]. The extent and severity of drug resistance is expected to increase in the coming years [10,11], creating the need to determine optimal treatment strategies to minimize the problem.

A common strategy that physicians use to avoid drug resistance is combining multiple drugs [12,13]. Combination therapies target multiple biological mechanisms of a pathogen, reducing the likelihood of developing resistance to all drugs combined. When resistances occur, physicians typically replace the therapy [4,14,15]. However, stochastic effects can play a role in the detection of resistance [16,17], the management of adverse effects [4,18], or the introduction of new drugs in the market [19]. Therefore, to fully understand the problem, we need to simultaneously account for the stochastic effects in therapy switching and the multiple components of combination therapy.

Mathematical models have been used to emulate drug resistance at different scales. At a cellular level, these models have been used to study how multiple metabolic mechanisms of a pathogen affect its growth and level of resistance [20]. At the host level, host-pathogen interactions have also been modeled to study competition and trade-offs that lead to resistances [21–23]. At the population level, mathematical models have been used to assess the effectiveness of public health strategies, such as hygiene protocols, surveillance, and regulating the use of antimicrobial drugs [24–26].

In contrast to previous models, our goal is to develop a stochastic model that identifies optimal strategies of administering therapies to a host, namely, combination therapy and

*Contact author: edgar@ictp.it

†Contact author: daniel.sanchez@unibe.ch

Published by the American Physical Society under the terms of the Creative Commons Attribution 4.0 International license. Further distribution of this work must maintain attribution to the author(s) and the published article's title, journal citation, and DOI.

therapy switching [12–15]. In doing so, we present a two-scale model that describes the efficacy of therapies administered to a host. The first scale accounts for pathogenic evolution, which results in changes in the therapy efficacy. This evolution is a direct consequence of pathogenic mutation which is inherently stochastic [27,28]. The second scale accounts for host-pathogen dynamics of a chronic infection, such as HIV-1 [22,29] and is linked to the first scale via the infection rate, which depends on the current therapy efficacy.

In this study, pathogenic evolution is modeled in two ways. First, we employed a diffusion process in multiple dimensions, where each component of the position vector of the process represents the efficacy of a drug, and therapy changes are modeled using the framework of stochastic resetting [30,31], which has found recent applications in biology [32–35]. While a faithful representation of evolutionary dynamics should bear the discreteness of genomic changes [28], continuous approximations of these dynamics are also used [36] to ease the analysis. The efficacy space also includes a region representing therapy failure. Typically, stochastic resetting problems aim to minimize the first-passage time [37–41], but the need to maximize this time emerges naturally in our model, as the first-passage time is equivalent to the drug resistance development time [42].

Resistance emerges from rare mutants that expand under treatment; therefore, modeling population heterogeneity is essential to accurately capture this process [21–23,43–45]. To investigate this phenomenon, we implemented a second approach that includes single-cell heterogeneity as follows: Infected cells are grouped into mutation states, each with a different susceptibility to treatment. As the infection progresses, random mutations cause transitions of infected cells between these states. Then, the overall efficacy is calculated as the average mutation state across the population, which is then compared with the efficacy of our first model.

The paper is organized as follows: We first discuss the specifications of the model (Sec. II). Then we analyze the dependence of the model on its parameters (Sec. III) and the effect of imposing restrictions on the number of administered therapies (Sec. IV). We then introduce a more realistic model that accounts for heterogeneity to study the robustness of our results (Sec. V). Finally, we summarize and discuss our results (Sec. VI).

II. MULTIDRUG STOCHASTIC MODELS

In this section, we present our model for resistance development, along with the variables and assumptions underlying our study. Our primary goal is to investigate how drug resistance develops in patients undergoing treatment. A major challenge is that drug resistance dynamics results from the interaction of biological processes across multiple scales. The first scale involves the host cells infected by the pathogen, which we model as a compartmental ordinary differential equation (ODE). The second scale involves the evolution dynamics of the pathogen, which we model as a drifted diffusion.

To model the host cell and pathogen dynamics, we use an adapted compartmental framework for chronic infections, specifically HIV-1 [22,29]. The model categorizes cells into three states: healthy (H), latently infected (L), and actively infecting (I):

$$\begin{aligned}\dot{H} &= \alpha - \lambda_H H - \beta H I(1-\eta),\\ \dot{L} &= \epsilon\beta H I(1-\eta) + pL - \frac{pL^2}{K} - a_L L - \lambda_L L,\\ \dot{I} &= (1-\epsilon)\beta H I(1-\eta) + a_L L - \lambda_I I.\end{aligned} \tag{1}$$

H cells are incorporated into the system with a constant rate of α and die at a rate of $\lambda_H H$. The infection of H is characterized as a law of mass action with the form $w(H, L+I \to H-1, L+I+1) = \beta HI(1-\eta)$, where η is the therapy efficacy. Upon infection, cells transition into L cells with probability ϵ, or I cells with probability $1-\epsilon$. L cells proliferate following a logistic growth, constrained by carrying capacity K at a rate $pL(1-(L/K))$, and die with a rate $\lambda_L L$. Finally, L cells can activate with a rate aL resulting in I cells, and I cells die with a rate of $\lambda_I I$. All the parameter values are provided in Table I.

The parameter η determines the efficacy of a therapy being administered to a host. To account for simultaneous therapies [12,13], we replace $\beta HI(1-\eta)$ with $\beta HI\prod_{i=1}^{N_T}(1-\eta_i)$, following the framework for independently acting therapies [46–48]. Hence, the host-pathogen model that considers N_T therapies would be

$$\begin{aligned}\dot{H} &= \alpha - \lambda_H H - \beta H I\prod_{i=1}^{N_T}(1-\eta_i),\\ \dot{L} &= \epsilon\beta H I\prod_{i=1}^{N_T}(1-\eta_i) + pL - \frac{pL^2}{K} - a_L L - \lambda_L L,\\ \dot{I} &= (1-\epsilon)\beta H I\prod_{i=1}^{N_T}(1-\eta_i) + a_L L - \lambda_I I.\end{aligned} \tag{2}$$

A therapy efficacy of $\eta_i = 1$ signifies a perfect therapy, as it removes the infection rate. On the other hand, $\eta_i = 0$ refers to an absorbing boundary and signifies a complete failure of the therapy as it maximizes the rate. The value of each η_i depends on various factors which can vary over time due to mutations [27]. For this reason, we consider each therapy efficacy to be a stochastic process, $\eta_i \to \eta_t(t)$. The two scales are linked by an infection rate, which determines the number of infected cells in the host-pathogen model, and it is reduced by the therapy efficacy, similar to previous models [22,23,29].

It is known that pathogenic evolution is influenced by more stochastic effects and has slower dynamics than the host-pathogen interactions [27,28]. Hence, we choose to focus on the scale of therapy efficacy fluctuations, driven by pathogen evolution, while the host-pathogen dynamics are assumed to be at the steady state. Mathematically, this timescale separation implies that we explicitly consider the time dependence of each $\eta_i(t)$, while H, I, and L are treated as functions of the model parameters and therapy efficacies, without explicit time dependence. We refer readers to Appendix A for the expressions of the fixed points for healthy, infectious, and latent cells.

Another essential ingredient of our model is the inclusion of therapy switching. When a therapy is switched with a different one, the pathogens are exposed to a new stimulus and must restart the drug resistance development process. We

TABLE I. Table of parameters in Fig. 1(c), adapted from a within-host model of HIV-1 [22,29,42]. Values H_0, L_0, and I_0 were obtained with Eq. (A1) given $N_T = 2$, $\eta_1 = \eta_2 = 0.8$.

Parameter	Description	Value	Unit
H_0	Initial H population	599 326	cells/mL
L_0	Initial L population	45	cells/mL
I_0	Initial I population	11	cells/mL
α	Rate of H recruitment	6000	cells/(mL day)
λ_H	H death rate constant	0.01	1/day
η_i	Efficacy of the ith therapy	varies	
N_T	Number of therapies	varies	
β	Infection rate constant	5×10^{-6}	mL/day
ϵ	Fraction of infections yielding $H \to L$	0.01	
$1-\epsilon$	Fraction of infections yielding $H \to I$	0.99	
p	L proliferation rate constant	0.2	1/day
K	Carrying capacity of L cells	100	cells/mL
a_L	Activation rate constant of L cells	0.1	1/day
λ_L	L death rate constant	0.01	1/day
λ_I	I death rate constant	1	1/day

model such switches as abrupt changes of therapy efficacies at random times, thus making use of the stochastic resetting framework [30,31]. There are various inherently stochastic effects that influence therapy switching, e.g., the detection of resistance [16,17], adverse effects [4,18], or new drugs on the market [19].

Summing up, we describe the evolution of the multitherapy efficacy as a stochastic process; in particular, we use a multivariate stochastic differential equation (SDE) to describe therapy evolution between therapy switches:

$$\mathrm{d}\eta_i = \begin{cases} \eta_i(0) - \eta_i(t) & \text{if } t \in \chi_i, \\ \mu_i(\eta_i, t)\mathrm{d}t + \sqrt{2D}\,\mathrm{d}W_i(t) & \text{otherwise,} \end{cases} \tag{3}$$

where the index i refers to the ith therapy out of N_T therapies, η_i is the efficacy of the ith therapy, μ_i is a drift function, D is diffusivity, and $W_i(t)$ is a Wiener process. Pathogenic evolution favors mutations with stronger resistances to improve the survival [27]; therefore, we assume that the drift vector is biased toward therapy failure, $\mu_i < 0$. At certain random times, the therapy efficacy returns to its initial value, signifying a therapy switch. These therapy switching times are taken from a sequence $\chi_i = \{t^*_{i,1}, t^*_{i,2}, \ldots\}$, whose elements are partial sums of independent and identically-distributed exponential random variables, i.e. $t^*_{i,j} - t^*_{i,j-1} \sim \mathrm{Exp}(\tau_i)$, with mean $1/\tau_i$, which is the therapy switching rate for the ith therapy.

Equation (3) is supplemented with reflecting and partially absorbing boundary conditions. If one of the therapy efficacies reaches zero, $\eta_i = 0$, it remains at zero until a therapy switch triggers a reset, $\eta_i \to \eta_i(0)$. The absorbing boundary signifies that the pathogen has mutated to a point where it has fully lost the mechanism at which the therapy is targeting, giving it total resistance [20]. On the other hand, a reflecting boundary is placed at $\eta = 1$, ensuring the system does not enter regions where therapy effectiveness exceeds 100%. Equation (3) assumes that the discrete changes in the genome of the pathogen are small enough to be considered continuous [36], but, to assess the robustness of this assumption, we also consider a discrete-space model.

Figures 1(a) and 1(b) illustrate all the stochastic events included in our model for therapy efficacy evolution of a treatment involving two therapies ($N_T = 2$). Event 1 represents the therapy onset, where the initial therapy efficacy sets the efficacy level after therapy switches. Event 2 signals the effect of the reflecting boundary. Event 3 shows the effect of when both therapies have a low efficacy. Event 4 shows the effect of therapy switches. Event 5 demonstrates the impact of the partially absorbing boundary, which halts the evolution of one therapy's efficacy until a therapy switch reactivates it (event 6). Overall, the evolution is tracked until the number of healthy cells decreases below a certain threshold (event 7).

The impact of changes in therapy efficacy on the number of healthy cells during one therapy cycle is shown schematically in Fig. 1(b). The number of healthy cells at the fixed point as a function of η_1 and η_2 is shown in Fig. 1(c). We note that it is not necessary for all N_T therapies to reach complete failure for the host to be in a critical state characterized by a low level of healthy cells due to an infection of a drug-resistant pathogen. Indeed, in Fig. 1(c) we begin to see a decrease in the number of healthy cells even for $\eta_1, \eta_2 > 0$. Hence, we consider that the therapy efficacy is below a certain threshold for drug resistance to occur. In this work, we define $\sqrt{\sum_{i=1}^{N_T} \eta_i^2} \leqslant \eta_{\min}$ as an approximation for the condition for drug failure, with $\eta_{\min} = 0.4$.

By modeling the fluctuations of therapy efficacies due to evolution, we aim to obtain approximations to the time at which drug resistance occurs, which we define as the *resistance development time* (RDT). This quantity is synonymous with the first-passage time, defined as the time at which the stochastic process $\sqrt{\sum_{i=1}^{N_T} \eta_i^2(t)}$ first reaches the threshold state $\eta_{\min}$ [49].

Solving the RDT statistics associated with SDE (3) together with stochastic switching and boundary conditions is challenging due to the geometry of the boundary conditions. Standard techniques to solve this equation are not known to be effective [49–52]. We instead propose two models of an N_T-dimensional fluctuating therapy efficacy with therapy switching that are analogous to the model explained so

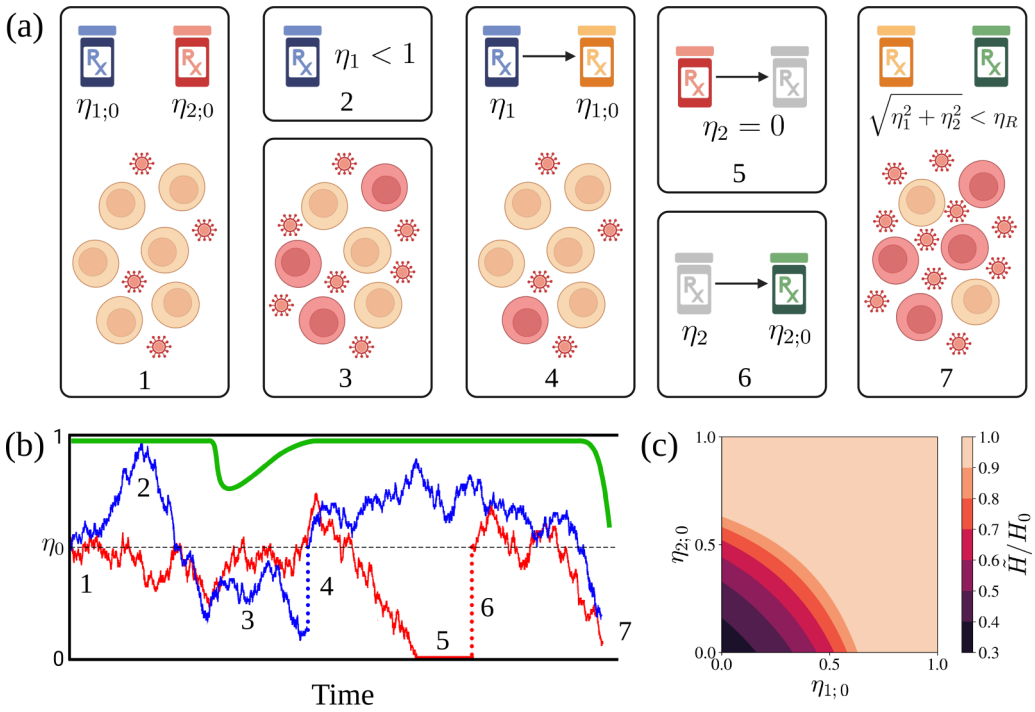


FIG. 1. Schematic representation of the two-scale mathematical model of drug resistance development in terms of the efficacy of an antimicrobial therapy. (a) A diagram showing the host-pathogen scale for two therapies, illustrating how drug resistance emerges and the impact of therapy changes. (b) Illustration of a stochastic trajectory of the efficacies of two therapies (in blue and red) and the normalized number of healthy cells (H/H_0, in green), showing the events described in panel (a): (1) The initial value of therapy efficacy is shown as a black horizontal dashed line. (2) The therapy efficacy is bounded by a reflecting boundary at $\eta = 1$. (3) Healthy cells drop due to a decrease in efficacy of both therapies. (4) Switching one of the therapies. (5) *Partial* absorption due to one of the therapies failing, which does not decrease the healthy population due to the effect of the other therapy. (6) Switching the failed therapy. (7) Failure of both therapies, leading to a decrease in the healthy cells to a critical level. (c) Normalized number of healthy cells at equilibrium as a function of the therapy efficacies, showing the existence of a critical region when both efficacies are low. The analytical expression for the equilibrium of H is computed in Appendix A and within-host model parameters are found in Table I.

far, but that exploit symmetries and approximations in the space spanned by the therapy efficacy. The first method is a continuous-space model that reduces the dynamics of the multidimensional SDE which allows for the calculation of analytical expressions of the mean RDT. The second method is a discrete-space model that explicitly shows the dynamics of the model and produces all statistical quantities of the RDT.

A. Coupled Continuous Model

Our initial approach is to consider a coarser model that tracks only the evolution of overall therapy efficacy, defined as an effective radius $\eta = \sqrt{\sum_{i=1}^{N_T} \eta_i^2}$. Since the absorbing boundary representing therapy failure exhibits rotational symmetry [see Fig. 1(c)], we can simplify the computation of first-passage-time averages when the drift term in Eq. (3) also respects this symmetry. Following the change of variables described in Appendix B, and using a particular form of the rotational-invariant drift (i.e., the same drift coefficient for all therapies), Eq. (3) reduces to

$$\mathrm{d}\eta = \frac{\tilde{v}}{\eta}\mathrm{d}t + D\mathrm{d}W(t), \tag{4}$$

where $\tilde{v} = D[N_T - 1 - (v/D)]$ is an effective drift that depends explicitly on the number of dimensions, N_T. Therefore, the imposed symmetry respects the absorbing boundary in Fig. 1(c), while allowing us to study the efficacy evolution of a therapy with an arbitrary number of drugs, while using a one-dimensional process in Eq. (4). In this simplified description, every therapy switch affects simultaneously all different therapies. A schematic of this model is found in Fig. 2(a) for $N_T = 2$. Using the formalism of the backward Fokker-Planck equation, we derive an analytical expression for the mean RDT conditioned to an initial efficacy η [51,53],

$$\langle T|\eta\rangle = \tau\,\frac{Y_d(-\mathrm{i}\overline{\eta}_{\max})[J_{d-1}(-\mathrm{i}\overline{\eta}) - (\eta/\eta_{\min})^{d-1}J_{d-1}(-\mathrm{i}\overline{\eta}_{\min})] + J_d(-\mathrm{i}\overline{\eta}_{\max})[Y_{d-1}(-\mathrm{i}\overline{\eta}) - (\eta/\eta_{\min})^{d-1}Y_{d-1}(-\mathrm{i}\overline{\eta}_{\min})]}{J_d(-\mathrm{i}\overline{\eta}_{\max})Y_{d-1}(-\mathrm{i}\overline{\eta}) - Y_d(-\mathrm{i}\overline{\eta}_{\max})J_{d-1}(-\mathrm{i}\overline{\eta})}. \tag{5}$$

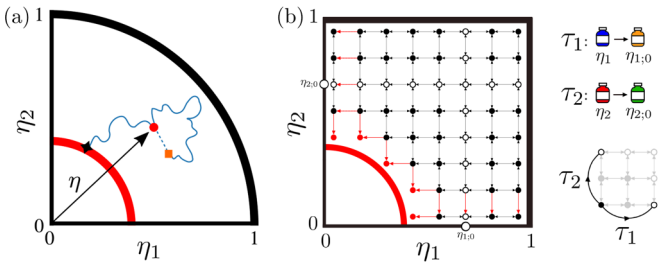


FIG. 2. Sketch of the coupled and uncoupled models for $N_T = 2$ for the efficacy of two drugs. (a) The coupled continuous model, with rotational symmetry and η as the distance from the origin. The trajectories start at the initial efficacy (dot), upon a therapy switch (square) the therapy efficacy goes back to the initial position, and the process stops when it reaches the absorbing region (star). (b) The uncoupled discrete model forms a lattice of $M \times M$ states, where each state corresponds to a value of the efficacy. Changes in therapy efficacy are transitions from one state to an adjacent state. Red states represent the absorbing states of the model. Upon a therapy switch in the ith therapy, the system returns to the points labeled in white, $\eta_{i;0}$. Efficacy $\eta_i = 1$ represents reflecting boundaries and $\eta_i = 0$ represents partially absorbing boundaries.

Here, J_n and Y_n are the Bessel functions of order n of the first and second kind, respectively, and $d = 2[(v/D) + N_T]$, where $(v/D) + N_T$ can be interpreted as an effective dimension of the efficacy space. We also introduced rescaled efficacies $\overline{\eta} = \lambda\eta$, $\overline{\eta}_{\min} = \lambda\eta_{\min}$, with $\lambda = (D\tau)^{-1/2}$ and $\overline{\eta}_{\max} = \lambda\eta_{\max}$, with $\eta_{\min}$ and $\eta_{\max}$ as the scaled radial locations of the absorbing and reflecting boundary, respectively. The characteristic scale λ is the inverse of the typical length traveled by genetic diffusion before a therapy switch occurs. See Appendix B for the derivation of Eq. (5) and further mathematical details.

B. Uncoupled Discrete Model

In the second model of drug resistance, we model the discrete phenotypic changes of a pathogen undergoing mutation [28] as a chain of states. We assume that the chain of states is equally spaced with M states, such that $\eta_i = j/M$, for $j = 0, \ldots, M-1$ and $i = 1, \ldots, N_T$. Transition rates control the evolution of η_i on the chain: rate p_i refers to an increase $\eta_i \to \eta_i + 1/M$, rate q_i refers to a decrease $\eta_i \to \eta_i - 1/M$, and rate $1/\tau_i$ refers to a therapy switch $\eta_i \to \eta_{i;0}$. This model independently evolves and switches the therapy efficacy for all N_T therapies.

For simultaneous therapies, we form a vector of therapy efficacies $\boldsymbol{\eta} = (\eta_1, \ldots, \eta_{N_T})^\top$, which is interpreted as an ordered coordinate, generalizing the chain of M states to an N_T-dimensional lattice of $M^{N_T} \times M^{N_T}$ states. A sketch of how this model is constructed is in Fig. 2(b) for $N_T = 2$. Transitions between states on this lattice can be written as a transition matrix $\mathbf{W}$, and the evolution of the vector $\boldsymbol{\eta}$ is controlled by a master equation

$$\frac{\mathrm{d}p(\boldsymbol{\eta}, t)}{\mathrm{d}t} = \mathbf{W}p(\boldsymbol{\eta}, t), \tag{6}$$

where $p(\boldsymbol{\eta}, t)$ is a column vector of probabilities tracking all N_T therapy efficacies at each time. For any two efficacy states on the lattice, $\boldsymbol{\eta}_a$ and $\boldsymbol{\eta}_b$, $\mathbf{W}$ has positive elements W_{ba} referring to the transition rates from state $\boldsymbol{\eta}_a$ to $\boldsymbol{\eta}_b$, and negative diagonal elements $W_{bb} = -\sum_{a \neq b} W_{ba}$ referring to the escape rates from state $\boldsymbol{\eta}_b$. Further details about the construction of the transition matrix $\mathbf{W}$ are found in Appendix C. This formulation of the model also allows us to utilize simulation methods such as the Gillespie algorithm to generate the trajectories of $\boldsymbol{\eta}$ [54].

To compare the change in state space from continuous to discrete, we obtained an approximate SDE for the uncoupled model using a Kramers-Moyal expansion [53,55]. This relates the discrete transition rates p_i and q_i to the continuous parameters v_i and D_i. The approximated SDE is a version of the general SDE in Eq. (3) but where each of the N_T therapies evolves independently of one another:

$$\mathrm{d}\eta_i = -v_i\mathrm{d}t + \sqrt{2D_i}\mathrm{d}W_i(t), \tag{7}$$

for $1 \leqslant i \leqslant N_T$. The details of the approximation and how v_i and D_i relate to the discrete transition rates p_i and q_i are found in Appendix C 1.

We recall that the RDT is computed by taking the time at which the overall therapy efficacy $\sqrt{\sum_{i=1}^{N_T} \eta_i^2}$ reaches below $\eta_{\min} = 0.4$. For this model, this condition is imposed by removing states and transitions on the lattice that fall below this boundary, which consequently means that the transition matrix $\mathbf{W}$ is modified. The details for this modification are found in Appendix C 2.

We now obtain the mean RDT for a discrete space of states, following the method outlined in Refs. [56–59]. Let η, η_a, and η_i refer to states on the lattice. Specifically, η_a is a state along the absorbing boundary, η is the initial state $\eta \equiv (\eta_1^{(0)}, \ldots, \eta_{N_T}^{(0)})$, and η_i is any state on the lattice that is neither η nor η_a. The mean time at which the therapy efficacy reaches an absorbing state η_a starting from the initial state η at time t is

$$\langle T|\eta\rangle = \sum_{\forall(\eta_i \to \eta_a)} [\mathbf{W}^\top]_{\eta_a,\eta_i}[(\mathbf{S}^{-1})^2]_{\eta_i,\eta}, \tag{8}$$

where we sum over all single-step transitions that lead to the absorbing boundary $(\eta_i \to \eta_a)$, $\forall \eta_i \neq \eta_a$. The matrix $\mathbf{S}$ is called the *survival* matrix, equal to $\mathbf{W}$ with transition elements $(\eta \to \eta_a)$ set to zero, as discussed in Refs. [56–59].

III. RESISTANCE DEVELOPMENT TIME AS A FUNCTION OF THERAPY ADMINISTRATION STRATEGIES

Simultaneous therapies are known to induce nonlinear effects, complicating the assessment of overall therapy efficacy [48]. Therefore, in this section, we aim to determine the impact of multiple therapies and switches on therapy efficacy dynamics, specifically their effects on the mean RDT.

A. Switching rates and number of therapies may lead to detrimental effects

We first consider a scenario where therapy efficacies are interdependent, and therapy switches affect all therapies simultaneously. This situation is well represented by the coupled model described in Sec. II A, which enables us to investigate therapy efficacy evolution for an arbitrary number of therapies. In Fig. 3, we plot the mean RDT conditioned

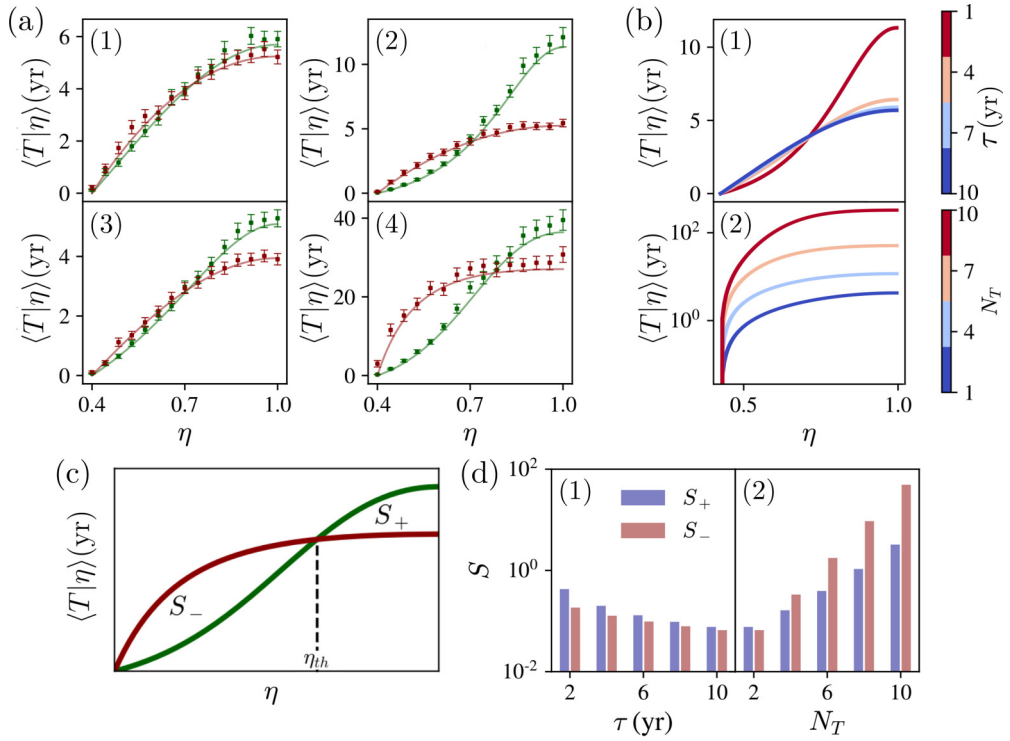


FIG. 3. Effect of number of therapies (N_T), switching times (τ), and initial therapy efficacy (η) in the mean RDT. (a) Mean RDT with and without therapy resets (green and red, respectively) as a function of initial therapy efficacy for (a1) $\tau = 10$ yr and $N_T = 2$, (a2) $\tau = 1$ yr and $N_T = 2$, (a3) $N_T = 1$ and $\tau = 3$ yr, and (a4) $N_T = 6$ and $\tau = 3$ yr. The plot illustrates that drug resistance times are more sensitive to therapy switching as the number of therapies increases and switching times decrease. While switching extends resistance times when initial therapy efficacy is high, it shortens them when initial efficacy is low. (b) Mean RDT as a function of η for different values of the switching times (b1) and number of therapies (b2), underscoring their roles as critical independent parameters. (c) An illustration of the curves for the mean RDT as a function of initial therapy efficacy with and without therapy switching, highlighting the intersection of the curves η_{th}, which define the boundaries of S_+ and S_-. (d) Differences between the areas under the curve before (red) and after (blue) η_{th} (d1) as a function of τ with $N_T = 2$ and (d2) as a function of N_T and fixed $\tau = 3$ yr. The regions where therapy switching is detrimental (S_-) or beneficial (S_+) expand with increasing number of therapies and switching rate, highlighting the potential benefit of switching when $\eta > \eta_{\mathrm{TH}}$ and its risk when $\eta < \eta_{\mathrm{TH}}$. Parameters: $v = -8 \times 10^{-5}$ days^{-1} and $D = 10^{-4}$ days^{-1}. In all panels solid lines were obtained with Eq. (5), while dots and error bars are sample means and the standard error computed from 10^3 Euler-Maruyama simulations of the process.

on the initial therapy efficacy, $\langle T|\eta\rangle$, using the coupled model for therapies with and without drug switching. By comparing the mean RDT with and without therapy switching, we can assess whether therapy switches are detrimental or beneficial in terms of maximizing the mean RDT. Figures 3(a1) and 3(a2) show that there is an increase in the overall differences between the curves of switching and nonswitching as the average time between therapy switches (τ) decreases. Similarly, Figs. 3(a3) and 3(a4) show an increase in the difference between the two curves as N_T increases. This difference increase is consistent for any τ or N_T, as shown by the analytical results in Figs. 3(b1) and 3(b2).

We can always identify a threshold in the initial therapy efficacy, η_{th}, that marks the transition between a region where therapy switches are beneficial ($\eta > \eta_{th}$), in the sense that therapy switches tend to increase the RDT, and another region in which therapy switches are detrimental ($\eta < \eta_{th}$), as shown in the sketch of Fig. 3(c). To quantify the relevance of the beneficial and detrimental areas, the area between the mean RDT curves with and without therapy switches is computed for $\eta_{th} \leqslant \eta < 1$, which we call S_+, and $0 \leqslant \eta < \eta_{th}$, called S_-. The intersection η_{th} together with the areas S_- and S_+ is illustrated in Fig. 3(c). Figures 3(d1) and 3(d2) show that S_+ and S_- decrease with increasing τ, but the opposite happens for increasing N_T. We also note that S_- increases faster than S_+ when increasing N_T. This suggests that patients undergoing multidrug therapies are at risk of experiencing significant detrimental effects, in the sense of a decrease in their mean RDT, due to therapy switches.

The remaining parameters of the coupled model, v and D, do not introduce any new phenomena beyond what is already captured by τ and N_T (see details in Appendix B 2). Therefore, we identify N_T and τ as independent and relevant parameters for therapy efficacy dynamics.

B. Determining the probability of detrimental therapy change protocols

So far we have observed that applying therapy switches simultaneously across all therapies can lead to detrimental effects, specifically by accelerating the development of drug resistance. In this section, we assess whether this undesirable effect persists when drug switches are applied independently. Additionally, we estimate the probability that therapies

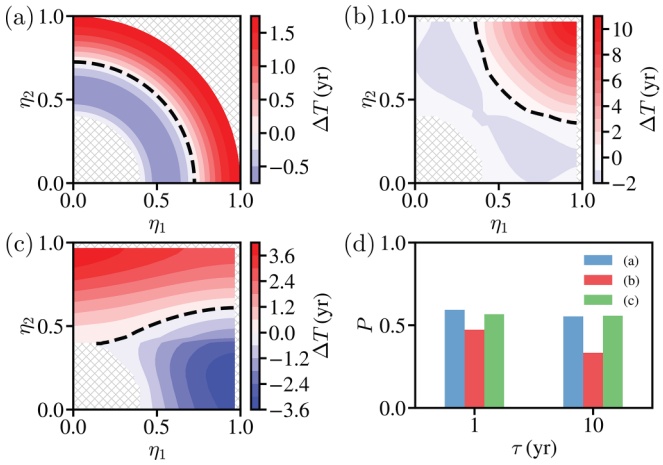


FIG. 4. Impact of therapy protocol on the risk associated with therapy switching. Difference between the mean RDT with therapy switching and without therapy switching (ΔT) as a function of initial therapy efficacy for (a) the coupled continuous model, (b) uncoupled discrete model with switching allowed for both therapies, and (c) uncoupled discrete model with switching allowed only for one drug η_1. Dashed lines indicate the region where the mean RDTs coincide. These panels illustrate that extended regions where therapy switching is beneficial or detrimental always exist, but their shape and extent depend critically on the type of switching protocol. (d) The fraction occupied by the initial therapy states that the mean RDT with switching is higher than without switching (P) as a function of τ. This fraction serves as a proxy for the probability that therapy switching is beneficial for patients. While coupled and uncoupled therapies exhibit similar risks when switching affects both therapies, the risk increases when switching affects only one of the therapies. Parameters: $\tau = 3$, $N_T = 2$, $v = -8 \times 10^{-5}$ days^{-1}, and $D = 10^{-4}$ days^{-1}.

involving drug switches may increase the risk of resistance development in patients.

In Fig. 4, we calculate the difference in mean RDT with and without therapy switching,

$$\Delta T = \langle T|\eta\rangle - \langle T|\eta\rangle_0, \tag{9}$$

for all possible combinations of initial therapy efficacies involving two therapies ($N_T = 2$) and switching all therapies at the same time or individually. Figure 4(a) shows that switching therapies at the same time has beneficial effects when the initial efficacies are far from the boundary, consistent with the results in Fig. 3. In Fig. 4(b), we observe qualitatively similar behavior using the uncoupled model [Eq. (8)], which allows us to study the development of drug resistance when therapies evolve and switch independently. The uncoupled model allows for switching to be done for only one of the two therapies, as shown in Fig. 4(c). In this nonsymmetrical scenario, the beneficial and detrimental regions now produce a nontrivial gradient. In summary, there are parameter regions where drug switching is detrimental whether therapies are switched simultaneously or individually. Moreover, the detrimental areas can have complex shapes, as shown in Fig. 4(c).

Figure 4(d) shows that the percentage of space occupied by the beneficial region (called P). This quantity is of interest because it refers to the probability that the therapy design is beneficial for patients, assuming the initial therapy efficacies $\boldsymbol{\eta}$ are uniformly distributed. The beneficial region does not vary much as the switching rate is increased for both the coupled model and for the case of the uncoupled model where only one therapy is allowed to be switched. However, this is not the case for switching both therapies with an equal rate.

IV. LIMITING THERAPIES REVEALS OPTIMAL STRATEGIES

In the previous section, we showed that therapy switches can have both positive and negative effects on resistance development. For this reason, we aim to identify therapy administration strategies that minimize resistance development. A trivial solution to maximize the RDT is to choose an infinite therapy switching rate or an infinite number of simultaneous therapies. However, infinite therapies are not feasible in a realistic clinical scenario, since the number of therapies available to patients is limited. In this section, we study therapy strategies that maximize the RDT, under the practical constraints of limited therapy switching and imposed therapy costs.

We begin by fixing the number of simultaneous therapies to $N_T = 2$ and study the mean RDT as a function of the therapy switching rate. Let ℓ represent the number of allowed switches, so that therapy switching is no longer permitted after the ℓth switch. The mean RDT is obtained using simulations of the uncoupled discrete model, which evolves over time without imposing a coupling between therapies. Trajectories of the uncoupled model are generated with the Gillespie algorithm [60] using the transition matrix $\mathbf{W}$ as defined in Eq. (6). In Fig. 5(a), we reveal a nonmonotonic behavior for the mean RDT as the switching rate is varied. This suggests that, given a limited number of therapies available, there is an optimal therapy switching rate that will maximize the mean RDT.

Next, we fix the switch rate τ while varying the number of simultaneous therapies, N_T. In this case, we use the coupled continuous model, which allows for more simultaneous therapies but imposes simultaneous therapy switching. In this model, a single allowed therapy switch $\ell = 1$ with $N_T = 2$ drugs would require four drugs in total, while two allowed switches $\ell = 2$ with $N_T = 3$ would require nine drugs. To account for the realistic scenario where the total number of drugs used throughout the therapy is limited, we fix the total number of drugs involved, denoted by A_T. Therefore, for a fixed A_T, the number of allowed switches will depend on N_T as follows:

$$\ell = \frac{A_T}{N_T} - 1. \tag{10}$$

The mean RDT for this version of limited switching is computed using simulations of the coupled continuous model using the Euler-Maruyama algorithm [60] of the SDE in Eq. (4). Here we see a change in the dependence of the mean RDT with D: from an increasing behavior for a larger D to a decreasing behavior for a smaller D. The diffusion constant D controls how much therapy efficacy fluctuates over time and therefore it should grow with the mutation rate of the infecting pathogen. Figure 5(b) suggests that pathogens that mutate slower (i.e., smaller D) benefit from fewer simultaneous therapies and more limited switches, while the opposite is true for faster mutating pathogens.

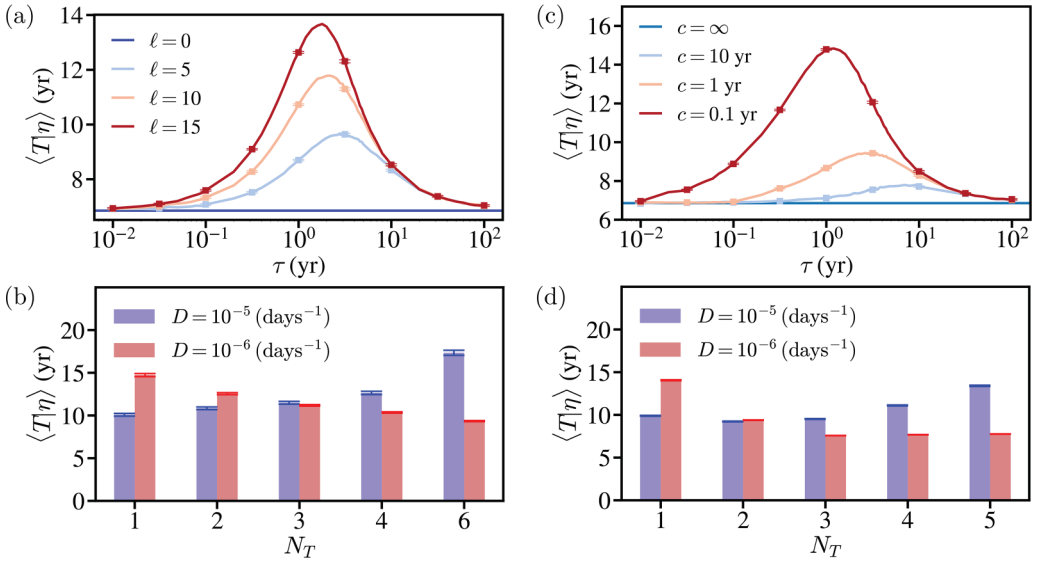


FIG. 5. Optimal therapy design considering a maximum number of switches and associated therapy costs. (a) Mean RDT with limited switching as a function of τ for different values of the maximum number of switches (ℓ). This panel illustrates the existence of an optimal switching time maximizing the mean RDT. (b) Mean RDT with limited switching as a function of N_T for two values of D. The maximum number of switches is fixed through Eq. (10) using $A_T = 12$. Here we show that the benefit of increasing the number of drugs in a therapy depends on the strength of the efficacy diffusion. (c) Mean RDT with costed switching as a function of τ and for different values of the parameter cost (c). (d) Mean RDT with costed switching as a function of N_T for two values D. In both (c) and (d) we use the cost parameter $c = 10^{N_T-1}$. The results derived from costed switching are equivalent to those of limited switching changing the role of ℓ by c. Graphs in (a) and (c) were generated using the uncoupled discrete model, while the effect of the number of drugs in (b) and (d) was inspected with the continuous coupled model. Parameters: $v = -8 \times 10^{-5}$ days^{-1} and 10^6 simulations each point.

In addition to fixing the number of therapies, we study the impact of a cost for each switch. We model this cost by using a therapy switching rate that makes subsequent switches less frequent [61,62]. Let γ be the number of therapies that have been administered at a certain time. We replace the therapy switching rate with a function,

$$C(\gamma) = \frac{1}{\tau} \exp\left(-\frac{c}{\tau}\gamma\right), \tag{11}$$

where c is a cost parameter that represents the average time taken for new therapies to be made available to the host, and τ is the time between therapy switches without cost. Lower cost parameters c allow for more switching in a shorter amount of time, emulating a limit in the therapies. Therefore, the cost function in Eq. (11) ensures that successive switches in the therapy $\gamma \to \infty$ diminish the therapy switching rate $1/\tau \to 0$. With this constraint, there is still an optimal switching rate that maximizes the RDT, as shown in Fig. 5(c), similar to Fig. 5(a).

To analyze how costs affect the mean RDT as the number of therapies varies (using the coupled model), we modify the cost function, Eq. (11), by using a cost parameter that is dependent on N_T: $c = 10^{N_T-1}$. This ensures that increasing the number of simultaneous therapies in the coupled model also increases the cost of each switch. In Fig. 5(d), we show the RDT for two values of D in the coupled model with switching costs.

Figure 5(d) suggests that more simultaneous therapies, although costlier, are beneficial for more volatile infections with large D, and vice versa for small D.

V. SINGLE-CELL HETEROGENEITY

Our models so far have assumed that mutations occur simultaneously and homogeneously among all pathogens within the host. This simplification enabled us to define the effective homogeneous coupled and uncoupled models, and to study the evolution of therapy efficacy using a single variable, η. In this section, we verify that the main results derived from the effective models in Sec. II also hold a more detailed model that incorporates explicit mechanisms of pathogen evolution. We refer to this more complex model as the *single-cell heterogeneous model*.

The single-cell heterogeneous model explicitly considers drug resistance as the outcome of mutations occurring at the individual level—where a single mutant pathogen may arise and spread if it outcompetes the others. Specifically, instead of modeling therapy efficacy η as a diffusion process, as in Eq. (3), we stratify the latently infected (L) and actively infecting (I) cell populations into $S + 1$ discrete mutation states: L_i and I_i for $i = 0, \ldots, S$. Each mutation state is associated with specific mutation rates and a corresponding therapy efficacy $\eta_i = i/S$.

Figure 6(a) illustrates the relevant reactions that the heterogeneous model considers. For simplicity, we assume that only a single therapy is being administered, $N_T = 1$. We note that the majority of the interactions, e.g., infection of the susceptible cells, activation of latently infected cells, etc., are the same as in Eq. (1), but emphasize that these interactions happen only within the same mutation state i. We assume mutations to occur only upon the proliferation of latently infected cells L_i with a base rate pL_i. We now introduce two

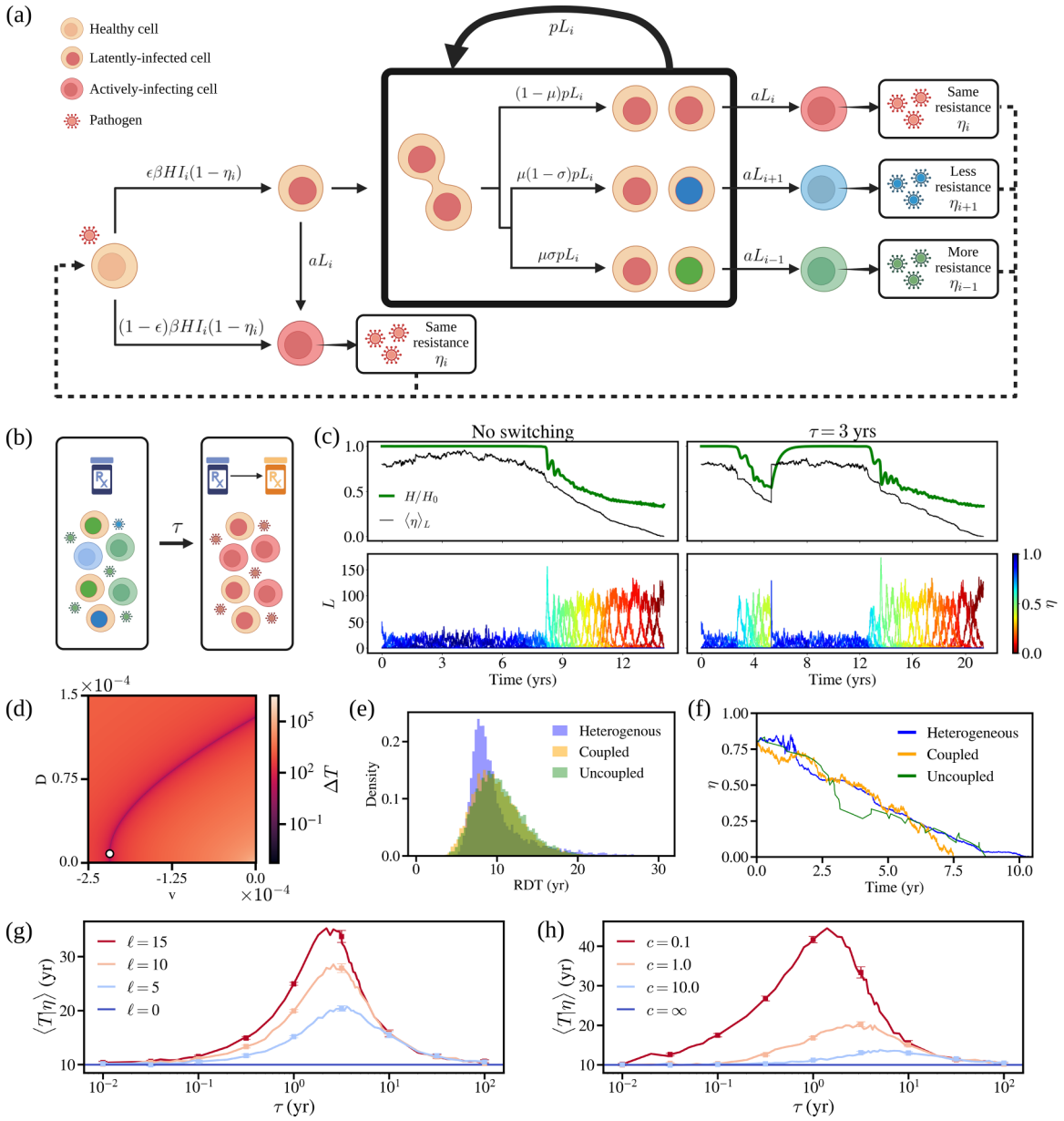


FIG. 6. Parameter estimation and robustness analysis were performed using the single-cell heterogeneity model. (a) Sketch of the expanded mechanisms included in the heterogeneous model, along with their transition rates coming from mutation state i. See Appendix D for full mathematical details. (b) A sketch shows the impact of therapy switching within the heterogeneous model. (c) Representative trajectories of healthy cells and the average therapy efficacy (top), and of the latently infected cell population (bottom). The left column shows evolution without therapy switching, while the right column includes switching. Latently infected cell trajectories are color coded by mutation state. (d) The absolute difference between the mean RDT between the heterogeneous model and the SDE in Eq. (13) as a function of v and D. The white circle indicates the point with the smallest absolute mean difference and lowest analytical variance. Optimal parameters: $v^* = -2.18 \times 10^{-4}$ days^{-1}, $D^* = 8.1 \times 10^{-6}$ days^{-1}. (e) Comparison of RDT distributions obtained from the heterogeneous model, homogeneous coupled model, and homogeneous uncoupled model using the optimized parameters v^* and D^* from (d), with 10^5 simulations for all models. (f) Sample trajectories from all three models. (g) Mean RDT with limited switching as a function of τ for different allowed numbers of therapies ℓ using the heterogeneous model. (h) Mean RDT with costed switching as a function of τ for different cost parameters c using the heterogeneous model. Parameters: $S = 30$ mutation states, $\mu = 0.05$ mutation probability, $\sigma = 0.5$ state transition probability, $M = 30$ efficacy states, $p^* = 4.02 \times 10^{-3}$ days^{-1}, $q^* = 1.06 \times 10^{-2}$ days^{-1}. Parameters for the uncoupled model were computed using Eq. (C3).

parameters: mutation probability μ and state transition probability σ. Proliferation of L_i may generate an L_i, L_{i+1}, or L_{i-1} cell, with rates $(1-\mu)pL_i$, $\mu\sigma pL_i$, and $\mu(1-\sigma)pL_i$, respectively. These mutant latent cells will eventually activate to be an actively infecting cell of the type I_i, I_{i+1}, or I_{i-1}, respectively, which have a corresponding constant therapy efficacy η_i, η_{i+1}, and η_{i-1}. Appendix D outlines the mathematical form of this model.

Therapy changes exposes all the cells and pathogens to a new stimulus. Therefore, we model therapy switching with

rate τ as an abrupt reset of the mutation states of the total L_i and total I_i are transferred to its initial state, as illustrated in Fig. 6(b). The mathematical details of a therapy switch are also found in Appendix D. Figure 6(c) shows simulated trajectories of the healthy and latently infected cell populations with and without therapy switches.

The overall therapy efficacy experienced by the host is computed as the average of η_i weighted by the number of corresponding L_i at each time:

$$\langle \eta_i \rangle_L = \frac{\sum_{i=0}^{S} \eta_i L_i}{\sum_{i=0}^{S} L_i}. \tag{12}$$

Resistances are assumed to have developed entirely when $\langle \eta_i \rangle_L$ has reached zero, denoting that both latently infected and actively infecting cells are infected with a pathogen that is fully resistant against the therapy. Note that in Fig. 6, the state transition probability is $\sigma = 0.5$, denoting an equal probability for a mutated proliferation to yield a mutant with either more or less resistance. It is due to selection that the model shows a bias toward lower values of drug resistance.

A. Parametrizing the diffusion model using single-cell heterogeneity

We first parametrize the drift-diffusion model using the trajectories of the therapy efficacy generated by the heterogeneous model, denoted by $\langle \eta \rangle_L$. Figure 6(c) shows that $\langle \eta \rangle_L$ fluctuates much like how η fluctuates when it is governed by a drift-diffusion process. Thus, we propose that there are optimal parameters used in the drift-diffusion model that exist which closely match the statistics of the heterogeneous model. We let v^* and D^* be these optimal drift and diffusion constants.

The estimation of the optimal parameters of the drift-diffusion model is done by evaluating the absolute value between the difference of the means:

$$\Delta T = |\langle T \rangle_H - \langle T | \eta_0 \rangle_A|, \tag{13}$$

where $\langle T \rangle_H$ is the mean RDT of the heterogeneous model, and $\langle T | \eta_0 \rangle_A$ is the mean RDT of the SDE in Eq. (3),

$$\mathrm{d}\eta = v\mathrm{d}t + \sqrt{2D}\,\mathrm{d}W(t). \tag{14}$$

This SDE is also bounded by the absorbing and reflecting conditions that were described in Sec. II. The mean RDT for this SDE was derived in Refs. [42,63], in the context of first-passage times.

In Fig. 6(d) we evaluate ΔT [Eq. (13)] as a function of v and D of the drift-diffusion model. As expected, there are multiple combinations of (v, D) that minimize ΔT. However, the analytical variance of the SDE in Eq. (14) was also derived in Refs. [42,63]. The parameter values that produced the lowest analytical variance are chosen as the v^* and D^*, and best match the statistics of the heterogeneous model [open white circle in 6(d)].

Figure 6(e) shows the direct comparisons of the RDT distribution of the heterogeneous model, and the homogeneous coupled and uncoupled models using the optimal v^* and D^*. Furthermore, Fig. 6(f) compares sample trajectories of the heterogeneous model, and homogeneous coupled and uncoupled models. The coupled model RDTs and trajectories have been simulated using the Euler-Maruyama algorithm, and the heterogeneous and uncoupled model have both been simulated using the Gillespie algorithm.

B. Single-cell heterogeneity does not change optimal therapy change strategies

Next, we impose limitations on the number of therapies that may be replaced in the single-cell heterogeneity model. Limits are imposed by counting the number of therapy switches within the model, and if the number exceeds a limit ℓ, switching can no longer be performed. On the other hand, costs are imposed by replacing the constant therapy switching rate with the function in Eq. (11), characterized by a parameter γ which is the number of therapies that have been administered and switched at a given time, and c which is proportional to the amount of time that therapies are made available to the patient. Figures 6(g) and 6(h) show that imposing either a limit or cost reveals an optimal therapy switching rate that maximizes the RDT. This result is qualitatively similar to what was shown with the SDE (homogeneous) model in Sec. IV. This allows us to assess the robustness of the homogeneous model.

VI. DISCUSSION

In this work, we have presented and characterized a stochastic model to study therapy administration strategies that aim to reduce drug resistance development. In particular, we have identified how therapy switches and the combination of therapies impact the resistance development time with and without restrictions on drug availability. We have also introduced a more complex model that considers single-cell heterogeneity.

Our model has extended previous results of stochastic models of therapy administration [42] by accounting for multiple therapies administered to the host which are known to induce nonlinear changes in the overall therapy efficacy [48]. We considered a therapy efficacy that scales the rate of infection in a host-pathogen model of HIV-1 dynamics, allowing us to study chronic diseases [22,29]. Typically, therapy efficacy is included in the models as a constant rate or a functional form for the rate of infection and mutation [20,22,23,29,64]. However, drug resistance can be modeled as a stochastic process [65], allowing our model to account for temporal changes in therapy efficacy due to the noisy effects of pathogenic evolution. We have presented two models to study this phenomenon, namely, the coupled continuous model and the uncoupled discrete model. The coupled continuous model eases the analytical study, but it has more limitations. On the other hand, the uncoupled discrete model allows for a more realistic study of the process, but it is computationally expensive.

In cases of therapies with higher initial therapy efficacies, both models have shown that increasing either the number of simultaneous therapies or the switching rate increases the mean RDT, consistent with the literature on combination and sequential therapies [14,66–72]. The models identified conditions, in terms of initial efficacy, for therapy switching to be beneficial or detrimental to patient outcomes. The detrimental

effect is observed in case studies where adverse effects have resulted from drug switching [19,73].

As an extension to the model, restrictions in terms of the availability of the therapy were included. This allows for the study of the optimal allocation of resources and treatment, which has been studied previously for chronic illnesses such as HIV [74–76]. The different restrictions that we have considered are a maximum therapy switching rate, limitations in the available therapies, and costs to therapy switching. These restrictions avoid unrealistic strategies such as an infinite therapy switching rate.

Furthermore, the model has been constrained to consider only a limited number of therapies available or an increasing cost for each switch. In this setting, we showed that there is an optimal therapy switching rate that maximizes the RDT. It has been shown that if the costs for treatment and diagnostic checkups are significant, then therapy switching without these diagnostic checkups may fare better for the patient compared to evenly spaced diagnostic checkups [76]. Our results for limited and costed therapy switching suggest the existence of optimal periods of when patients may undergo diagnostic checkups with a physician to reduce the risk of therapy failure while minimizing costs.

In addition to the therapy switching rate, another controllable variable is the number of simultaneous therapies. In this case, we found that for high values of the diffusion constant, the mean RDT increases with the number of therapies. On the other hand, lower diffusion constants decrease the mean RDT as a function of the number of therapies. Note that the diffusion constant varies with each pathogen since it is correlated to its mutation rate. Therefore, our results suggest that for smaller rates of mutation, fewer simultaneous therapies are beneficial, while the opposite is true for larger mutation rates.

Our model aims to reproduce drug resistance development. However, a limitation of our approach is due to the fact that resistance emerges through population heterogeneity, where rare clones expand under treatment pressure [43–45]. To validate our approach, we have developed a heterogeneous population model to assess the robustness of our results. Both models showed the same qualitative behavior, including the emergence of an optimal therapy switching time under limited resources.

While both models coincide with their results, the drift-diffusion model does not have the high computational requirements of the heterogeneous model, which facilitates the study of larger parameter ranges and the analytical study. However, the parameters of the heterogeneous model are easier to relate to biologically measurable parameters such as mutation rates and therefore they could be used to parametrize the model. Then, the values of v and D can be estimated as the values that better match the key statistics of the heterogeneous model. This parametrization allows to apply the simpler model to more realistic scenarios.

Currently our work only considers a model of drug interaction where drugs are considered to have independent modes of action within the host; hence, the overall therapy efficacy in the infection rate is expressed as a product $\prod_{i=1}^{N_T}(1-\eta_i)$ [46,47]. However, different modes of drug interactions may also suppress or amplify the overall therapy efficacy [66], which may potentially change the form of the therapy efficacy. These interactions may also be simultaneous or sequential [48], potentially leading to changes in the optimal reset rates that have been identified. Furthermore, data obtained from empirical models of drug resistance may be used to inform the model [77,78]. While our work aims to study antimicrobial resistance, the model can easily be adapted to study drug resistance and drug switching in chronic or long-term illnesses without a pathogenic vector, such as diabetes [79], chronic obstructive pulmonary disease (COPD) [80], and hypertension [81–83].

Taken together, our model of therapy efficacy shows that the brute force strategy of increasing the rate of therapy switches and the number of drugs in the therapy might not result in better outcomes. In contrast, we can identify balanced optimal therapy choices depending on resource constraints that physicians designing therapies might face. While measuring the precise interactions between drugs, pathogens, and hosts can be complex, we have demonstrated that pathogen properties—such as the symmetries of phenotype landscapes and mutation rates, which can be assessed through empirical methods [28]—provide valuable insights for combating antimicrobial resistance.

ACKNOWLEDGMENTS

This work was supported by the Ruth & Arthur Scherbarth Foundation and the UniBE ID (Grant No. 2021). JA acknowledges additional support from Agencia Estatal de Investigacin (AEI, MCI, Spain), Grant No. MCIN/AEI/10.13039/501100011033. Fondo Europeo de Desarrollo Regional (FEDER, UE) under Project APASOS (PID2021-122256NB-C21/C22). María de Maeztu Program for Units of Excellence in R&D, Grant No. CEX2021-001164-M. MUR – PRIN – NextGenerationEU - Project Title "Emergent Dynamical Patterns of Disordered Systems with Applications to Natural Communities" CUP 2022WPHMXK.

DATA AVAILABILITY

The source code (in python) for plotting the figures in this text is available on GitHub [84].

APPENDIX A: STEADY STATES OF THE HOST-PATHOGEN MODEL

In this section, we will show the steady states of a host-pathogen model in Eq. (2) which are used in the quarter-circle absorbing boundary condition described in Sec. II and Fig. 1(c).

We assume that the host-pathogen model is at equilibrium; hence, we solve for the fixed points of the model by setting each equation in Eqs. (2) equal to zero and solving for H, L, and I, which we now denote as $\widetilde{H}$, $\widetilde{L}$, and $\widetilde{I}$. We first obtain a trivial fixed point at $\widetilde{H} = \alpha/\lambda_H, \widetilde{L} = 0, \widetilde{I} = 0$ and a nontrivial fixed point given by the following:

$$\begin{aligned}\widetilde{H} &= \frac{\alpha}{\lambda_H + b\widetilde{I}},\\ \widetilde{L} &= \frac{[\lambda_I b\widetilde{I} + (\lambda_I\lambda_H - (1-\epsilon)b\alpha)]\widetilde{I}}{a_L(b\widetilde{I} + \lambda_H)},\\ \widetilde{I} &= S + T - \frac{x_2}{3x_1},\end{aligned} \tag{A1}$$

where

$$
\begin{aligned}
S &= \sqrt[3]{R+\sqrt{Q^3+R^2}},\\
T &= \sqrt[3]{R-\sqrt{Q^3+R^2}},\\
Q &= \frac{3x_1x_3-x_2^2}{ax_1^2},\\
R &= \frac{9x_1x_2x_3-27x_1^2x_4-2x_2^2}{54x_1^3},\\
x_1 &= -p\lambda_I^2b^2,\\
x_2 &= -(2p\lambda_Ibc-dKa_L\lambda_Ib^2),\\
x_3 &= \epsilon b^2\alpha Ka_L^2-pc^2+dKa_L\lambda_H-\lambda_Ib,\\
x_4 &= \epsilon b\alpha Ka_L^2\lambda_H+dKa_L\lambda_Hc,\\
b &= \prod_{i=1}^{N_T}(1-\eta_i)\beta,\\
c &= \lambda_I\lambda_H-(1-\epsilon)b\alpha,\\
d &= p-a_L-\lambda_L.
\end{aligned}
\tag{A2}
$$

The fixed point $\widetilde{H}$ is used to compute the diagram in Fig. 1(c), where $\widetilde{H}$ is computed for $N_T=2$ and varying η_1 and η_2. This maps the amount of healthy cells at equilibrium to the space of therapy efficacy.

The parameter values used to generate the diagram in Fig. 1(c) are given by Table I.

APPENDIX B: COUPLED MODEL

1. Model derivation

In this section we derive Eq. (4) from the main text. This derivation will be performed without stochastic resetting, since the SDE with resetting is readily obtained by adding the indicator functions with the process χ, as explained in Eq. (3). Consider a general time-homogeneous multidimensional SDE in the Îto sense,

$$\mathrm{d}\boldsymbol{\eta} = \boldsymbol{\mu}(\boldsymbol{\eta})\mathrm{d}t + \boldsymbol{\sigma}(\boldsymbol{\eta})\mathrm{d}\boldsymbol{W}(t). \tag{B1}$$

The Fokker-Planck representation of such a process reads

$$\partial_t\rho_t(\boldsymbol{\eta}) = -\nabla\cdot[\rho_t(\boldsymbol{\eta})\boldsymbol{\mu}(\boldsymbol{\eta})] + \nabla^2[\boldsymbol{\sigma}(\boldsymbol{\eta})\boldsymbol{\sigma}^\intercal(\boldsymbol{\eta})\rho_t]. \tag{B2}$$

The above equation is invariant under orthogonal transformations of the diffusion matrix. Indeed, let $\boldsymbol{S}$ be an orthogonal matrix such that $\boldsymbol{S}\boldsymbol{S}^\intercal = \boldsymbol{I}$; then the process

$$\mathrm{d}\boldsymbol{\eta} = \boldsymbol{\mu}(\boldsymbol{\eta})\mathrm{d}t + \boldsymbol{S}\boldsymbol{\sigma}(\boldsymbol{\eta})\mathrm{d}\boldsymbol{W}(t) \tag{B3}$$

is statistically indistinguishable from the process in Eq. (B1) as both of them have the same associated Fokker-Planck equation [51].

Let us reduce the generality of the equations presented so far to adapt to the kind of models studied in the main text. In particular, we study isotropic and constant diffusion matrices,

$$\boldsymbol{\sigma} = \sqrt{2D}\boldsymbol{I}. \tag{B4}$$

Also, for the case of the coupled model we consider that therapies interact in such a way that the drift in the efficacy space is rotationally invariant,

$$\boldsymbol{\mu}(\boldsymbol{\eta}) = \boldsymbol{\eta}f(\eta), \tag{B5}$$

with $\eta = \sqrt{\boldsymbol{\eta}\cdot\boldsymbol{\eta}}$. Thus, the resulting rotationally invariant SDE reads

$$\mathrm{d}\boldsymbol{\eta} = \boldsymbol{\eta}\,f(\eta) + \sqrt{2D}\,\mathrm{d}\boldsymbol{W}(t). \tag{B6}$$

The idea now is to do a change of variables to spherical coordinates with one radius η and N_T-1 angles $\phi_1,\ldots,\phi_{N_T-1}$ using Îto's rule [51,53]. By doing so, we find that the radial drift only depends on η:

$$\sum_{i=1}^{N_T}\partial_{\eta_i}\eta\,\mathrm{d}\eta_i + D\partial_{\eta_i}^2\eta\,\mathrm{d}t = \left(\eta f(\eta) + D\frac{N_T-1}{\eta}\right)\mathrm{d}t. \tag{B7}$$

The radial diffusion will, in principle, depend both on the radial and angular variables. However, it can be shown that there is always an orthogonal transformation $\boldsymbol{S}$ making the evolution for the radial component independent of the angular variables,

$$\mathrm{d}\eta = \left(\eta f(\eta) + D\frac{N_T-1}{\eta}\right)\mathrm{d}t + \sqrt{2D}\,\mathrm{d}W(t). \tag{B8}$$

Evolution tends to produce pathogens that are more resistant to the therapy, and consequently this means that the efficacy of the therapy will rapidly decrease. A minimal choice for the drift function f that describes this mechanism is

$$f(\eta) = -\frac{v}{\eta^2}. \tag{B9}$$

Introducing this choice for f in Eq. (B8) together with the possibility of experiencing stochastic resets, we obtain Eq. (4) of the main text.

We note that this section begins by assuming our model follows an Îto stochastic differential equation. However, similar manipulations to those presented here can be applied if the stochastic differential equation follows a different interpretation, such as that of Stratonovich or Hänggi-Klimontovich. The reason is that non-Îto processes can always be converted into an Îto process by adding an extra drift term according to the drift-correction formula [51,53].

2. Effect of parameters

In the main text we analyzed in detail the effect of the number of simultaneous drugs in the therapy (N_T) and the average frequency between therapy switches, τ, as a function of the mean RDT (see Fig. 3 in the main text). Nevertheless, the coupled model depends on two more parameters: the diffusion constant D and the constant v tuning the radial drift. On the one hand, v only appears in the coupled model as a subtraction to the number of simultaneous drugs. Therefore, we can analyze changes in the drift as effective changes in the number of therapies, N_T, which was properly analyzed. Indeed, our model with parameter choice $v = v_0 + \Delta v$ and $N_T = n_0$ produces the same results as realizations with $v = v_0$ and $N_T = n_0 - \Delta v/D$. Thus, no new phenomenology is expected when varying v. On the other hand, the last free parameter D is also not relevant as it can be absorbed through

a change of variables of the time. Thus, choices of D can be seen as choices of time units.

3. Mean resistance development times

The equation for conditioned mean RDT, $\langle T|\eta\rangle$, can be obtained using the backward Fokker-Planck equation formalism [51,53]. In particular, the backward Fokker-Planck operator associated to the coupled model in Eq. (4) follows the equation

$$D\frac{d-1}{\eta}\frac{\mathrm{d}}{\mathrm{d}\eta}\langle T|\eta\rangle + D\frac{\mathrm{d}^2}{\mathrm{d}\eta^2}\langle T|\eta\rangle + \frac{1}{\tau}(\langle T|\eta_r\rangle - \langle T|\eta\rangle) = -1, \tag{B10}$$

Where $d = v/D + N_T$, η is the initial efficacy of the therapy, and η_r is the efficacy right after therapy switch. Further details on the derivation of Eq. (B10) may be found in Refs. [30,37].

Using the change of variables $G(\eta) = -\langle T|\eta_r\rangle + \langle T|\eta\rangle$, Eq. (B10) becomes

$$\frac{\mathrm{d}^2}{\mathrm{d}\eta^2}G(\eta) + \frac{d-1}{\eta}\frac{\mathrm{d}}{\mathrm{d}\eta}G(\eta) + \frac{1}{\lambda^2}G(\eta) = -\frac{1}{D}, \tag{B11}$$

with $\lambda = \sqrt{\tau D}$. Equation (B11) has $G_p(\eta) = \tau$ as a particular solution. The changes of variable $\eta = i\lambda x$, and $G(x) = g(x)x^{-\frac{d}{2}}$ transform the homogeneous part of the equation for G in a Bessel equation,

$$x^2\frac{\mathrm{d}^2}{\mathrm{d}x^2}g(x) + x\frac{\mathrm{d}}{\mathrm{d}x}g(x) + (x-\beta^2)g(x) = 0, \tag{B12}$$

with $\beta = (d/2) - 1$. Therefore, the general solution for Eq. (B10) reads

$$\langle T|\eta\rangle = \eta^\beta[c_1 J_\beta(-i\bar{\eta}) + c_2 Y_\beta(-i\bar{\eta})] + \tau + c_3, \tag{B13}$$

With $\bar{\eta} = \eta/\lambda$. Two of the three unknown constants of Eq. (B13) are determined through the boundary conditions

$$\langle T|\eta\rangle(\eta_{\min}) = 0, \tag{B14}$$

$$\frac{\mathrm{d}}{\mathrm{d}\eta}\langle T|\eta\rangle|_{\eta=\eta_{\max}} = 0, \tag{B15}$$

where $\eta_{\min}$ and $\eta_{\max}$ are the radial locations of the absorbing and reflecting boundary, respectively. The third equation is provided by the self-consistent relation

$$\langle T|\eta_r\rangle = c_3. \tag{B16}$$

The resulting equation for the average absorption time with initial condition η and resetting state η_r reads

$$\begin{aligned}\frac{\langle T|\eta\rangle}{\tau} =& \frac{J_{\beta+1}(-i\bar{\eta}_{\max})}{Z(\eta_r)}\left(\left(\frac{\eta_r}{\eta_{\min}}\right)^\beta Y_\beta(-i\bar{\eta}_{\min}) + \left(\frac{\eta_r}{\eta}\right)^\beta Y_\beta(-i\bar{\eta})\right)\\ &- \frac{Y_{\beta+1}(-i\bar{\eta}_{\max})}{Z(\eta_r)}\left(\left(\frac{\eta_r}{\eta_{\min}}\right)^\beta J_\beta(-i\bar{\eta}_{\min}) + \left(\frac{\eta_r}{\eta}\right)^\beta J_\beta(-i\bar{\eta})\right),\end{aligned} \tag{B17}$$

with

$$\begin{aligned}Z(\eta) =& J_{\beta+1}(-i\bar{\eta}_{\max})Y_\beta\left(-i\frac{\eta}{\lambda}\right)\\ &- Y_{\beta+1}(-i\bar{\eta}_{\max})J_\beta\left(-i\frac{\eta}{\lambda}\right),\end{aligned} \tag{B18}$$

and $\bar{\eta} = \eta/\lambda$, $\bar{\eta}_{\max} = \eta_{\max}/\lambda$, and $\bar{\eta}_{\min} = \eta_{\min}/\lambda$. Equation (5) is obtained from Eq. (B17) by fixing the resetting state to be equal to the initial condition of the process, $\eta_r = \eta$.

APPENDIX C: DERIVATION OF UNCOUPLED MODEL

1. Markov chain transition rates

In this section, we will derive the transition rates p_i and q_i as outlined in Sec. II B. The transitions from one state to another can be written as a Master equation:

$$\begin{aligned}\frac{\mathrm{d}p(\boldsymbol{\eta},t)}{\mathrm{d}t} =& \sum_{i=1}^{N_T}\frac{1}{\tau_i}\delta(\eta_i - \eta_{i;0}) + p_i p\left(\eta_i - \frac{1}{M}, t\right)\\ &+ q_i p\left(\eta_i + \frac{1}{M}, t\right) - \left(p_i + q_i + \frac{1}{\tau_i}\right)p(\eta_i, t),\end{aligned} \tag{C1}$$

where $\eta_{i;0}$ is the initial therapy efficacy of the ith therapy and $\delta(\eta_i - \eta_{i;0})$ is a Dirac delta function centered at the displacement of the current efficacy from the initial efficacy, $\eta_i - \eta_{i;0}$. We note that this master equation is similar in form to the master equation presented in Ref. [30], but is generalized by considering a Markov process on a lattice.

Terms p_i and q_i are the Markov jump rates to adjacent states that respectively increase or decrease the therapy efficacy. Taking a Kramers-Moyal expansion to the above allows us to obtain a Fokker-Planck equation [53,55]. This is done by performing a second-order Taylor expansion on the terms in the master equation that are shifted by $1/M$. This expansion is performed such that the $1/M$ terms will be factored outside of the propagators, i.e., expanding $p(\eta_i + (1/M), \ldots, \eta_{N_T}, t)$ centered at $\eta_i + (1/M) = \eta_i$, $p(\eta_i - (1/M), \ldots, \eta_{N_T}, t)$ at $\eta_i - (1/M) = \eta_i$, and so on. Performing these expansions and simplifying,

$$\begin{aligned}\frac{\mathrm{d}p(\boldsymbol{\eta},t)}{\mathrm{d}t} =& \sum_{i=1}^{N_T}\frac{1}{\tau_i}\delta(\eta_i - \eta_{1;0}) - \frac{1}{\tau_i}p(\eta_i, t)\\ &- \frac{p_i - q_i}{M}\frac{\partial p(\eta_i,t)}{\partial \eta_i} + \frac{p_i + q_i}{2M^2}\frac{\partial^2 p(\eta_i,t)}{\partial \eta_1^2}\end{aligned} \tag{C2}$$

with the following effective drift and diffusion parameters:

$$v_i = \frac{p_i - q_i}{M}, \quad D_i = \frac{p_i + q_i}{2M^2}. \tag{C3}$$

Inverting these parameters,

$$\begin{aligned}p_i &= \tfrac{1}{2}(2D_iM^2 + v_iM),\\ q_i &= \tfrac{1}{2}(2D_iM^2 - v_iM),\end{aligned} \tag{C4}$$

We obtain the jump rates in the discrete space in terms of parameters used by the continuous space. As such, we are able to use the master equation formulation by constructing a transition matrix as discussed in the following section.

2. Generating the transition matrix

In this section, we will outline how the transition matrix for the uncoupled discrete model is generated to be used for the mean RDT formula in Eq. (8). Sums of transition rates p_i and q_i, and therapy switching rate $1/\tau_i$, occupy the elements of the transition matrix $\mathbf{W}$ in Eq. (6). In practice, to make the transition matrix $\mathbf{W}$, it is simpler to start with the transition matrix from a complete lattice graph, then add and remove nodes and edges as needed until we end up with the desired graph seen in Fig. 2(b).

Recall that the therapy efficacy vector $\boldsymbol{\eta}$ may be viewed as an ordered coordinate on an $M^{N_T} \times M^{N_T}$ lattice of states, where M is the number of therapy efficacy states for each therapy. Consider $N_T = 2$ therapies and two states $\boldsymbol{\eta}_a = (\eta_1^{(a)}, \eta_2^{(a)})$ and $\boldsymbol{\eta}_b = (\eta_1^{(b)}, \eta_2^{(b)})$.

We first form the transition matrix for the complete lattice graph $\mathbf{M}$ with matrix elements M_{ba} denoting a transition from state $\boldsymbol{\eta}_a$ to state $\boldsymbol{\eta}_b$. Element M_{ba} is equal to a transition rate p or q if states $\boldsymbol{\eta}_a$ and $\boldsymbol{\eta}_b$ are adjacent to each other on the lattice. This element is equal to transition rate p if the transition $\boldsymbol{\eta}_a \to \boldsymbol{\eta}_b$ increases exactly one therapy in $\boldsymbol{\eta}_a$ by $1/M$. On the other hand, this element is equal to q if the transition $\boldsymbol{\eta}_a \to \boldsymbol{\eta}_b$ decreases exactly one therapy in $\boldsymbol{\eta}_a$ by $1/M$. Diagonal elements of $\mathbf{M}$ are $M_{bb} = -\sum_{a\neq b} M_{ba}$ for each $b = 1, \ldots, M^2$. Any other matrix elements are zero.

Next, we form the transition matrix $\mathbf{R}$ that captures the behavior of therapy switching that returns the state back to its initial position. Let $\boldsymbol{\eta}_0 = (\eta_1^{(0)}, \eta_2^{(0)})$ be the initial state and $\boldsymbol{\eta}_b$ be any state that is not an initial state on a lattice generated by $\mathbf{M}$. Transition matrix $\mathbf{R}$ has elements R_{ba} that are equal to $1/\tau_1$ for all states $\boldsymbol{\eta}_b = (\eta_1^{(0)}, \eta_2^{(b)})$ and $1/\tau_2$ for all states $\boldsymbol{\eta}_b = (\eta_1^{(b)}, \eta_2^{(0)})$, for $b = 1, \ldots, M^2$. Diagonal elements of $\mathbf{R}$ are $R_{bb} = -\sum_{a\neq b} R_{ba}$ for each $b = 1, \ldots, M^2$. Any other matrix elements are zero.

We then form the transition matrix for partial absorption along the axes of the lattice, $\mathbf{P}$, signifying the failure of a single therapy with matrix elements P_{ba}. Element P_{ba} is equal to transition rate p if two states $\boldsymbol{\eta}_a$ and $\boldsymbol{\eta}_b$ are equal to $(0, \eta_2^{(a)})$ and $(1/M, \eta_2^{(b)})$, respectively, or $(\eta_1^{(a)}, 0)$ and $(\eta_1^{(b)}, 1/M)$, respectively. Here, states $\boldsymbol{\eta}_a$ are the states along the axis of the lattice, and $\boldsymbol{\eta}_b$ is the immediate adjacent state to $\boldsymbol{\eta}_a$ that is not another state on the axis, and the transitions refer to transitions $\boldsymbol{\eta}_a \to \boldsymbol{\eta}_b$. Similar to the previous two matrices, diagonal elements are $P_{bb} = -\sum_{a\neq b} P_{ba}$ for each $b = 1, \ldots, M^2$ and any other matrix elements are zero.

Finally, the transition matrix for complete absorption, $\mathbf{C}$, is formed by taking all states that fall below the absorbing condition $\sqrt{\sum_{i=1}^{N_T} \eta_i^2} \leqslant \eta_{\min}$ for $\eta_i \in \boldsymbol{\eta}_b$. Matrix elements C_{ba} are equal to M_{ba} if state $\boldsymbol{\eta}_b$ follow this condition.

These four matrices are added together to form the complete transition matrix $\mathbf{W}$ for $N_T = 2$,

$$\mathbf{W} = \mathbf{M} + \mathbf{R} - \mathbf{C} - \mathbf{P}. \tag{C5}$$

With this transition matrix, we may use expressions that are available to Markov chains [56–59] in computing for the RDT statistics, as discussed further in Sec. II B.

APPENDIX D: SINGLE-CELL HETEROGENEITY MODEL

In this section, we will show the mathematical details of the single-cell heterogeneity model. This model is analogous to the original host-pathogen model in Eq. (2) however, instead of coupling the therapy efficacy η with a stochastic differential equation in Eq. (3), we explicitly account for the mutation states as individual compartments in the ODE.

The compartments for latently infected cells L and actively infecting cells I are replaced with $S+1$ compartments each: L_i and I_i, where $i = 0, \ldots, S$. Each L_i and I_i contain a constant $\eta_i = i/S$ where $i = 0, \ldots, S$. Each state i refers to the level of drug resistance of the infecting pathogen, and consequently the efficacy of the therapy. For simplicity, we will use a single therapy $N_T = 1$ for this model:

$$\dot{H} = \alpha - \lambda_H H - \beta H \sum_{j=0}^{S} I_j(1-\eta_j), \tag{D1}$$

for $i = 0, 1$,

$$\dot{L}_i = \epsilon\beta H I_i - \lambda_L L_i - a_L L_i + (1-\mu)pL_i + \mu(1-\sigma)pL_{i+1} - \frac{pL_i}{K}\sum_{j=1}^{S} L_j, \tag{D2}$$

for $i = 2, \ldots, S-1$,

$$\dot{L}_i = \epsilon\beta H I_i(1-\eta_i) - \lambda_L L_i - a_L L_i + (1-\mu)pL_i + \mu\sigma pL_{i-1} + \mu(1-\sigma)pL_{i+1} - \frac{pL_i}{K}\sum_{j=0}^{S} L_j, \tag{D3}$$

$$\dot{L}_S = -\lambda_L L_S - a_L L_S + (1-\mu)pL_S + \mu\sigma pL_{S-1} - \frac{pL_S}{K}\sum_{j=0}^{S} L_j, \tag{D4}$$

for $i = 0, \ldots, S$,

$$\dot{I}_i = (1-\epsilon)\beta H I_i(1-\eta_i) + a_L L_i - \lambda_I I_i. \tag{D5}$$

The system of ODEs can be classified into the equation for the healthy cells [Eq. (D1)], the equations for the latently infected cells [Eqs. (D2)–(D4)], and the equation for the actively infecting cells [Eq. (D5)]. The equations for the latently infected cells are stratified into three based on the index i. Equation (D2) refers to the states at and close to the most resistant mutation strain, and is analogous to an absorbing boundary in the stochastic process version of the model. On the other hand, Eq. (D4) refers to the state at the least resistant strain and is analogous to a reflecting boundary in the stochastic process.

We also include therapy switching in this model, which involves summing all L_i and I_i right before a switching time $t^* \in \chi$, where χ was previously discussed in Eq. (3). Specifically, therapy switching follows the expressions

$$L_k(t^*) = \sum_{j=0}^{S} \lim_{t'\to t^{*-}} L_j(t'), \quad \text{and} \quad L_m(t^*) = 0, \tag{D6}$$

$$I_k(t^*) = \sum_{j=0}^{S} \lim_{t'\to t^{*-}} I_j(t'), \quad \text{and} \quad I_m(t^*) = 0, \tag{D7}$$

where $t^* \in \chi$ is a switching time, state k is the initial mutation state, and state m is any other state except k. The limit $\lim_{t' \to t^{*-}}(\cdot)$ is a left-sided limit approaching t^*, emphasizing that t' is the time immediately before the switching time t^*.

The model features similar rate parameters as in Eq. (2), with the addition of μ and σ which have been discussed in Sec. V. Furthermore, the carrying capacity of L_o are also summed over all possible combinations of products of L_i. The parameters used for these rates may be found in Table I.

[1] C. J. L. Murray *et al.*, Lancet **399**, 629 (2022).
[2] D. Liebenberg, B. G. Gordhan, and B. D. Kana, Front. Cell. Infect. Microbiol. **12**, 943545 (2022).
[3] A. N. Phillips, J. Stover, V. Cambiano, F. Nakagawa, M. R. Jordan, D. Pillay, M. Doherty, P. Revill, and S. Bertagnolio, J. Infect. Dis. **215**, 1362 (2017).
[4] K. H. Mayer, H. Drechsler and W. G. Powderly, Clin. Infect. Dis. **35**, 1219 (2002).
[5] N. Vasan, J. Baselga, and D. M. Hyman, Nature (London) **575**, 299 (2019).
[6] A. Catalano, D. Iacopetta, J. Ceramella, D. Scumaci, F. Giuzio, C. Saturnino, S. Aquaro, C. Rosano, and M. S. Sinicropi, Molecules **27**, 616 (2022).
[7] J. Maltas, D. S. Tadele, A. Durmaz, C. D. McFarland, M. Hinczewski, and J. G. Scott, PRX Life **2**, 023010 (2024).
[8] Y. Wu, X. Shi, X. Yao, and X. Du, Immun. Inflammation Dis. **11**, e850 (2023).
[9] N. R. Naylor, R. Atun, N. Zhu, K. Kulasabanathan, S. Silva, A. Chatterjee, G. M. Knight, and J. V. Robotham, Antimicrob. Resist. Infect. Control **7**, 58 (2018).
[10] J. O'Neill, *Tackling Drug-Resistant Infections Globally: Final Report and Recommendations* (Government of the United Kingdom, Wellcome Trust, London, 2016).
[11] B. J. Langford, M. So, M. Simeonova, V. Leung, J. Lo, T. Kan, S. Raybardhan, M. E. Sapin, K. Mponponsuo, A. Farrell *et al.*, Lancet Microbe **4**, e179 (2023).
[12] M. Baym, L. K. Stone, and R. Kishony, Science **351**, aad3292 (2016).
[13] M. Tyers and G. D. Wright, Nat. Rev. Microbiol. **17**, 141 (2019).
[14] V. I. Band, D. A. Hufnagel, S. Jaggavarapu, E. X. Sherman, J. E. Wozniak, S. W. Satola, M. M. Farley, J. T. Jacob, E. M. Burd, and D. S. Weiss, Nat. Microbiol. **4**, 1627 (2019).
[15] A. D. Haas, O. Keiser, E. Balestre, S. Brown, E. Bissagnene, C. Chimbetete, F. Dabis, M.-A. Davies, C. J. Hoffmann, P. Oyaro, R. Parkes-Ratanshi, S. J. Reynolds, I. Sikazwe, K. Wools-Kaloustian, D. M. Zannou, G. Wandeler, and M. Egger, Lancet HIV **2**, e271 (2015).
[16] O. Keiser, P. MacPhail, A. Boulle, R. Wood, M. Schechter, F. Dabis, E. Sprinz, and M. Egger, Trop. Med. Int. Health **14**, 1220 (2009).
[17] S. J. Reynolds, G. Nakigozi, K. Newell, A. Ndyanabo, R. Galiwongo, I. Boaz, T. C. Quinn, R. Gray, M. Wawer, and D. Serwadda, AIDS **23**, 697 (2009).
[18] I. Davidson, H. Beardsell, B. Smith, S. Mandalia, M. Bower, B. Gazzard, M. Nelson, and J. Stebbing, Antiviral Res. **86**, 227 (2010).
[19] M. G. Kirby, P. Allchorne, T. Appanna, P. Davey, R. Gledhill, J. S. A. Green, D. Greene, and D. J. Rosario, Int. J. Clin. Pract. **74**, (2019).
[20] F. Pinheiro, O. Warsi, D. I. Andersson, and M. Lässig, Nat. Ecol. Evol. **5**, 677 (2021).
[21] T. Lee, S. Bonhoeffer, and M. Penny, Results Phys. **34**, 105181 (2022).
[22] L. Rong and A. S. Perelson, PLoS Comput. Biol. **5**, e1000533 (2009).
[23] O. Sharomi and A. Gumel, J. Biol. Dyn. **2**, 323 (2008).
[24] A. M. Niewiadomska, B. Jayabalasingham, J. C. Seidman, L. Willem, B. Grenfell, D. Spiro, and C. Viboud, BMC Med. **17**, 81 (2019).
[25] H. Heesterbeek, R. M. Anderson, V. Andreasen, S. Bansal, D. De Angelis, C. Dye, K. T. D. Eames, W. J. Edmunds, S. D. W. Frost, S. Funk, T. D. Hollingsworth, T. House, V. Isham, P. Klepac, J. Lessler, J. O. Lloyd-Smith, C. J. E. Metcalf, D. Mollison, L. Pellis, J. R. C. Pulliam *et al.*, Science **347**, aaa4339 (2015).
[26] N. T. Hillock, T. L. Merlin, J. Turnidge, and J. Karnon, Appl. Health Econ. Health Policy **20**, 479 (2022).
[27] S. C. Manrubia, Curr. Opin. Virol. **2**, 531 (2012).
[28] A. Papkou, L. Garcia-Pastor, J. A. Escudero, and A. Wagner, Science **382**, eadh3860 (2023).
[29] A. P. Duncan Callaway, Bull. Math. Biol. **64**, 29 (2002).
[30] M. R. Evans and S. N. Majumdar, Phys. Rev. Lett. **106**, 160601 (2011).
[31] M. R. Evans, S. N. Majumdar, and G. Schehr, J. Phys. A: Math. Theor. **53**, 193001 (2020).
[32] T. Rotbart, S. Reuveni, and M. Urbakh, Phys. Rev. E **92**, 060101(R) (2015).
[33] É. Roldán, A. Lisica, D. Sánchez-Taltavull, and S. W. Grill, Phys. Rev. E **93**, 062411 (2016).
[34] A. Lisica, C. Engel, M. Jahnel, É. Roldán, E. A. Galburt, P. Cramer, and S. W. Grill, Proc. Natl. Acad. Sci. USA **113**, 2946 (2016).
[35] P. C. Bressloff, J. Phys. A: Math. Theor. **53**, 355001 (2020).
[36] J. Wang, K. Zhang, L. Xu, and E. Wang, Proc. Natl. Acad. Sci. USA **108**, 8257 (2011).
[37] M. R. Evans and S. N. Majumdar, J. Phys. A: Math. Theor. **44**, 435001 (2011).
[38] A. Pal and V. V. Prasad, Phys. Rev. E **99**, 032123 (2019).
[39] L. Kuśmierz and E. Gudowska-Nowak, Phys. Rev. E **92**, 052127 (2015).
[40] A. Pal and S. Reuveni, Phys. Rev. Lett. **118**, 030603 (2017).
[41] D. Das and L. Giuggioli, J. Phys. A: Math. Theor. **55**, 424004 (2022).
[42] A. Ramoso, J. Magalang, D. Sánchez-Taltavull, J. Esguerra, and E. Roldán, Europhys. Lett. **132**, 50003 (2020).
[43] R. Solé, J. Sardanyés, and S. F. Elena, Rep. Prog. Phys. **84**, 115901 (2021).
[44] M. A. Nowak and R. M. May, Math. Biosci. **106**, 1 (1991).
[45] M. A. Nowak, R. M. Anderson, M. C. Boerlijst, S. Bonhoeffer, R. M. May, A. J. McMichael, S. M. Wolinsky, K. J. Kunstman, J. T. Safrit, R. A. Koup, A. U. Neumann, and B. T. M. Korber, Science **274**, 1008 (1996).

[46] W. R. Greco, G. Bravo, and J. C. Parsons, Pharmacol. Rev. **47**, 331 (1995).
[47] C. I. Bliss, Ann. Appl. Biol. **26**, 585 (1939).
[48] R. Roemhild, T. Bollenbach, and D. I. Andersson, Nat. Rev. Microbiol. **20**, 478 (2022).
[49] S. Redner, *A Guide to First-Passage Processes* (Cambridge University Press, Cambridge, UK, 2001).
[50] D. L. Dy and J. P. Esguerra, Phys. Rev. E **88**, 012121 (2013).
[51] C. Gardiner, in *Stochastic Methods*, Springer series in synergetics (Springer, Berlin, 2008), pp. 1–22.
[52] L. Giuggioli, S. Sarvaharman, D. Das, D. Marris, and T. Kay, Multi-target search in bounded and heterogeneous environments: A lattice random walk perspective, *Target Search Problems* (Springer, 2024), pp. 107–133.
[53] N. G. V. Kampen, *Stochastic Processes in Physics and Chemistry* (Elsevier, Amsterdam, 2007).
[54] D. T. Gillespie, J. Phys. Chem. **81**, 2340 (1977).
[55] D. T. Gillespie, J. Chem. Phys. **72**, 5363 (1980).
[56] P. E. Harunari, A. Dutta, M. Polettini, and E. Roldán, Phys. Rev. X **12**, 041026 (2022).
[57] J. van der Meer, B. Ertel, and U. Seifert, Phys. Rev. X **12**, 031025 (2022).
[58] K. Sekimoto, arXiv:2110.02216.
[59] P. Jolakoski, A. Pal, T. Sandev, L. Kocarev, R. Metzler, and V. Stojkoski, Chaos Solitons Fractals **175**, 113921 (2023).
[60] R. Toral and P. Colet, *Stochastic Numerical Methods*, edited by R. Toral and P. Colet (Wiley, New York, 2014), Vol. 111, pp. 1009–1010.
[61] J. C. Sunil, R. A. Blythe, M. R. Evans, and S. N. Majumdar, J. Phys. A: Math. Theor. **56**, 395001 (2023).
[62] B. De Bruyne and F. Mori, Phys. Rev. Res. **5**, 013122 (2023).
[63] J. Magalang, R. Turin, J. Aguilar, L. Colombani, D. Sanchez-Taltavull, and R. Gatto, Phys. Rev. E **111**, 054117 (2025).
[64] S. Baral, R. Raja, P. Sen, and N. M. Dixit, WIREs Syst. Biol. Med. **11**, e1446 (2019).
[65] M. C. F. Prosperi, R. D'Autilia, F. Incardona, A. De Luca, M. Zazzi, and G. Ulivi, Bioinformatics **25**, 1040 (2009).
[66] D. I. Andersson, H. Nicoloff, and K. Hjort, Nat. Rev. Microbiol. **17**, 479 (2019).
[67] H. Nicoloff, K. Hjort, B. R. Levin, and D. I. Andersson, Nat. Microbiol. **4**, 504 (2019).
[68] R. Roemhild and H. Schulenburg, Evol. Med. Public Health **2019**, 37 (2019).
[69] C. E. H. Rosenkilde, C. Munck, A. Porse, M. Linkevicius, D. I. Andersson, and M. O. A. Sommer, Nat. Commun. **10**, 618 (2019).
[70] L. Imamovic and M. O. A. Sommer, Sci. Transl. Med. **5**, 204ra132 (2013).
[71] A. Batra, R. Roemhild, E. Rousseau, S. Franzenburg, S. Niemann, and H. Schulenburg, eLife **10**, e68876 (2021).
[72] M. Oette, E. Schülter, M. Rosen-Zvi, Y. Peres, M. Zazzi, A. Sönnerborg, D. Struck, A. Altmann, R. Kaiser, and the EuResist Network Study Group, Intervirology **55**, 160 (2012) .
[73] J. Sochman and M. Podzimkova, Int. J. Cardiol. **99**, 145 (2005).
[74] A. L. Avanceña and D. W. Hutton, Value Health **23**, 1509 (2020).
[75] M. L. Brandeau and G. S. Zaric, Health Care Manage. Sci. **12**, 27 (2009).
[76] S. Duwal, S. Winkelmann, C. Schütte, and M. von Kleist, PLoS Comput. Biol. **11**, e1004200 (2015).
[77] D. Chen, G. Liu, H. Du, J. Wee, R. Wang, J. Chen, J. Shen, and G.-W. Wei, ArXiv (2024).
[78] P. Lamirande, E. A. Gaffney, M. Gertz, P. K. Maini, J. R. Crawshaw, and A. Caruso, Invest. Ophthalmol. Vis. Sci. **65** (2024).
[79] H. E. Lebovitz and M. A. Banerji, Eur. J. Pharmacol. **490**, 135 (2004).
[80] F. Braido, F. Lavorini, F. Blasi, I. Baiardini, and G. W. Canonica, Int. J. Chronic Obstruct. Pulm. Dis. **2015**, 2601 (2015).
[81] M. C. S. Wong, W. W. S. Tam, C. S. K. Cheung, E. L. H. Tong, A. C. H. Sek, G. John, N. T. Cheung, B. P. Y. Yan, C. M. Yu, S. Leeder, and S. Griffiths, PLoS One **8**, e53625 (2013).
[82] J. Václavík, P. Vysočanová, J. Seidlerová, P. Zajíček, O. Petrák, J. Dlask, and J. Krýza, Medicine **93**, e168 (2014).
[83] V. G. Athyros, K. Tziomalos, A. Karagiannis, and D. P. Mikhailidis, Expert Opin. Pharmacother. **11**, 2943 (2010).
[84] https://github.com/jarmsmagalang/optimal_therapy_switching.